Supporting Information

Superior energy storage performance realized in antiferroelectric 0.10 wt% MnO_2-$AgNbO_3$ ceramics via Bi-doping induced phase engineering

Jing Wang,[‡a] Xuhui Fan,[‡ab] Zhen Liu,[‡c] Kongjun Zhu,[a] Hao Yuan,[ab] Zehan Zheng,[ab] Lei Zhao,[*d] Ji Zhang,[*c] Qibin Yuan[*e] and Jing-Feng Li[*f]

[a]*State Key Laboratory of Mechanics and Control for Aerospace Structures, College of Aerospace Engineering, Nanjing University of Aeronautics and Astronautics, Nanjing 210016, China*

[b]*School of Materials Science and Engineering, Nanjing University of Aeronautics and Astronautics, Nanjing 210016, China*

[c]*School of Materials Science and Engineering, Nanjing University of Science and Technology, Nanjing, 210094, China*

[d]*Key Laboratory of High-precision Computation and Application of Quantum Field Theory of Hebei Province, College Physics Science & Technology, Hebei University, Baoding 071002, China*

[e]*School of Electronic Information and Artificial Intelligence, Shaanxi University of Science and Technology, Xi'an, Shaanxi 710021, China*

[f]*State Key Laboratory of New Ceramics and Fine Processing, School of Materials Science and Engineering, Tsinghua University, Beijing, 100084, China*

[‡]These authors contributed equally to this work.

*Corresponding authors. E-mail addresses: leizhao@hbu.edu.cn (L. Zhao), jizhang@njust.edu.cn (J. Zhang), yuanqibin-sust@163.com (Q. B. Yuan), jingfeng@mail.tsinghua.edu.cn (J.-F. Li)

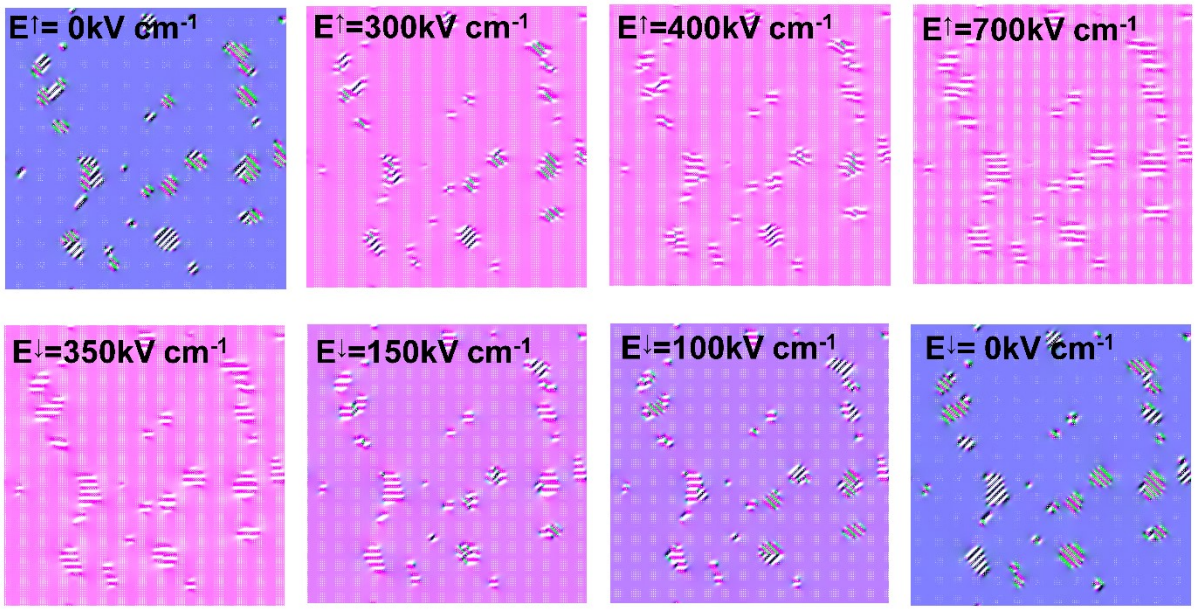

Fig. S1 The polarization switching behavior of the doped AN sample with 94% PE phase. E↑and E↓represent the stages of increasing electric field and decreasing electric field, respectively.

Fig. S1 indicates the polarization switching behavior of the doped AN sample with 94% PE phase. Upon increasing the electric field, the lamellar AFE domains gradually switch to the [001] direction and the structure transforms to FE state at 700 kV cm^{-1}. The FE state is maintained until the electric field decreases to 350 kV cm^{-1}. After that, it transfers back to local AFE domains.

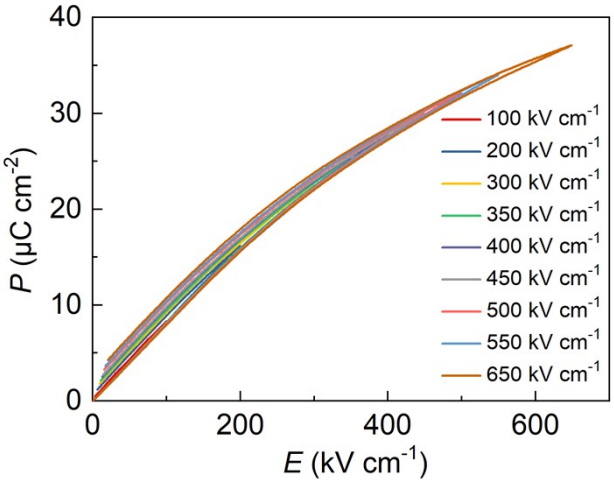

Fig. S2 Room-temperature *P-E* loops of AN-0.12Bi ceramic measured at various electric fields.

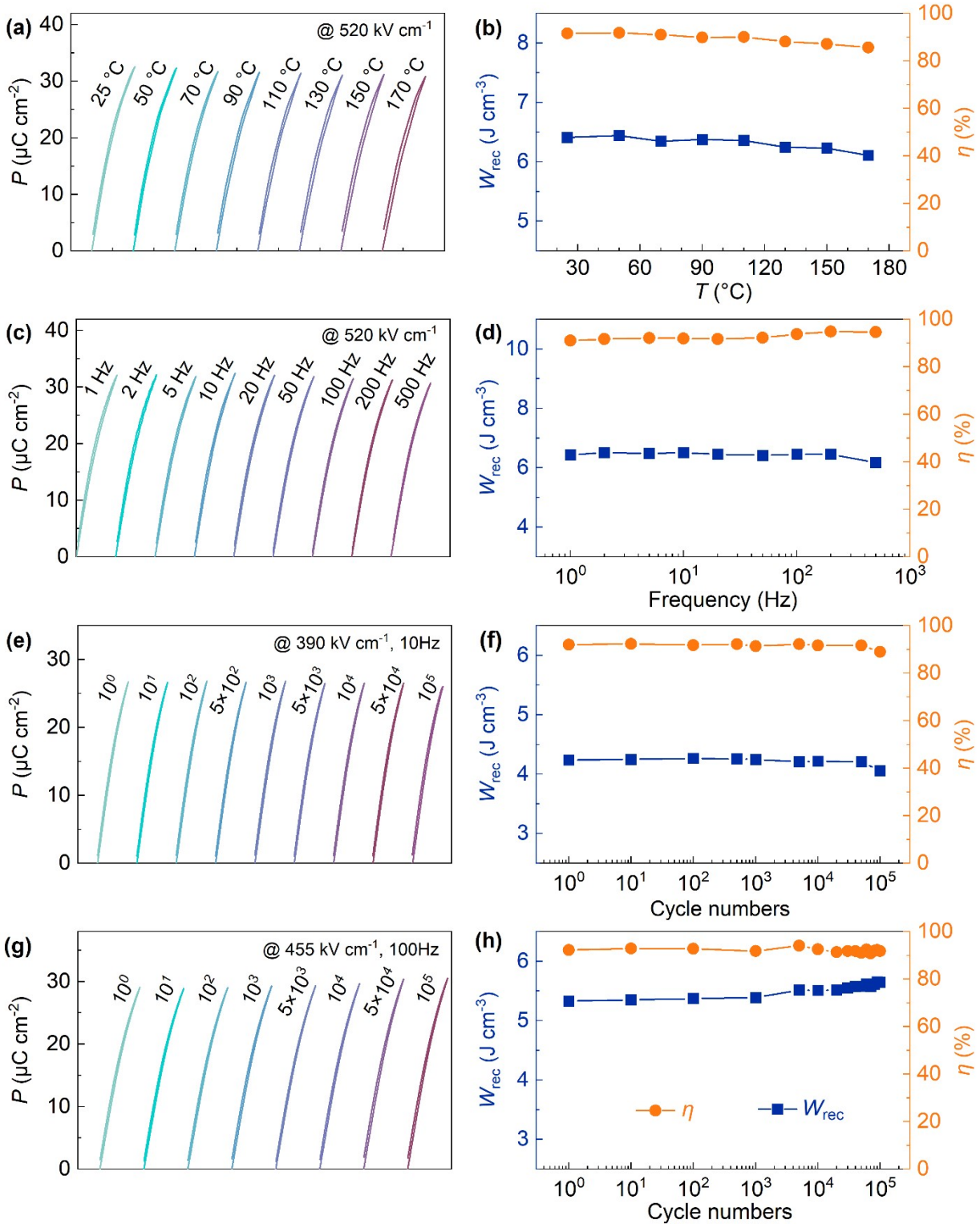

Fig. S3 (a)-(b)Temperature, (c)-(d)frequency and (e)-(h) cycling stability of AN-0.12Bi ceramic with (a)(c)(e)(g) *P*-*E* loops and (b)(d)(f)(h) corresponding W_{rec} and η.

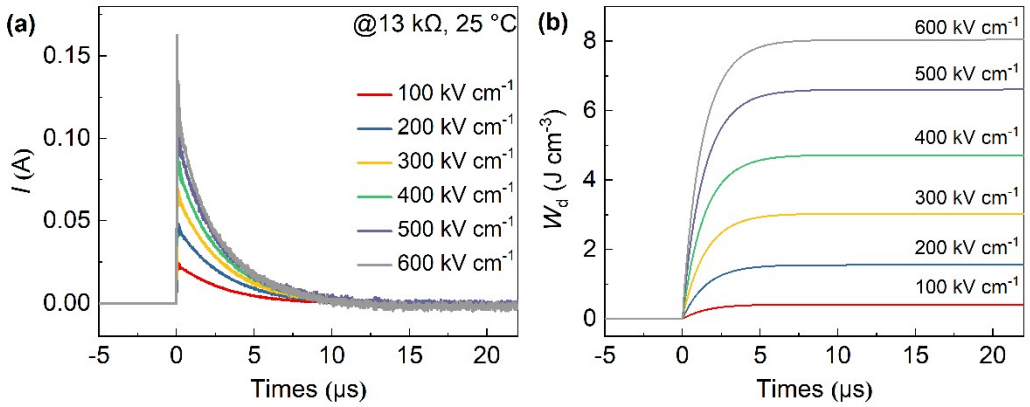

Fig. S4 The discharge (a) current-time curves and (b) W_d under different electric fields of the AN-0.12Bi ceramic.

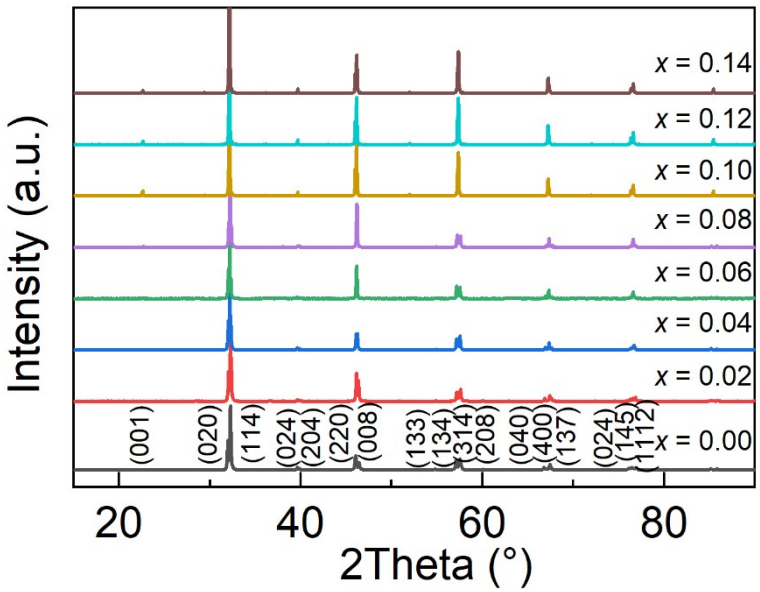

Fig. S5 XRD patterns of AN-*x*Bi ceramics at room temperature.

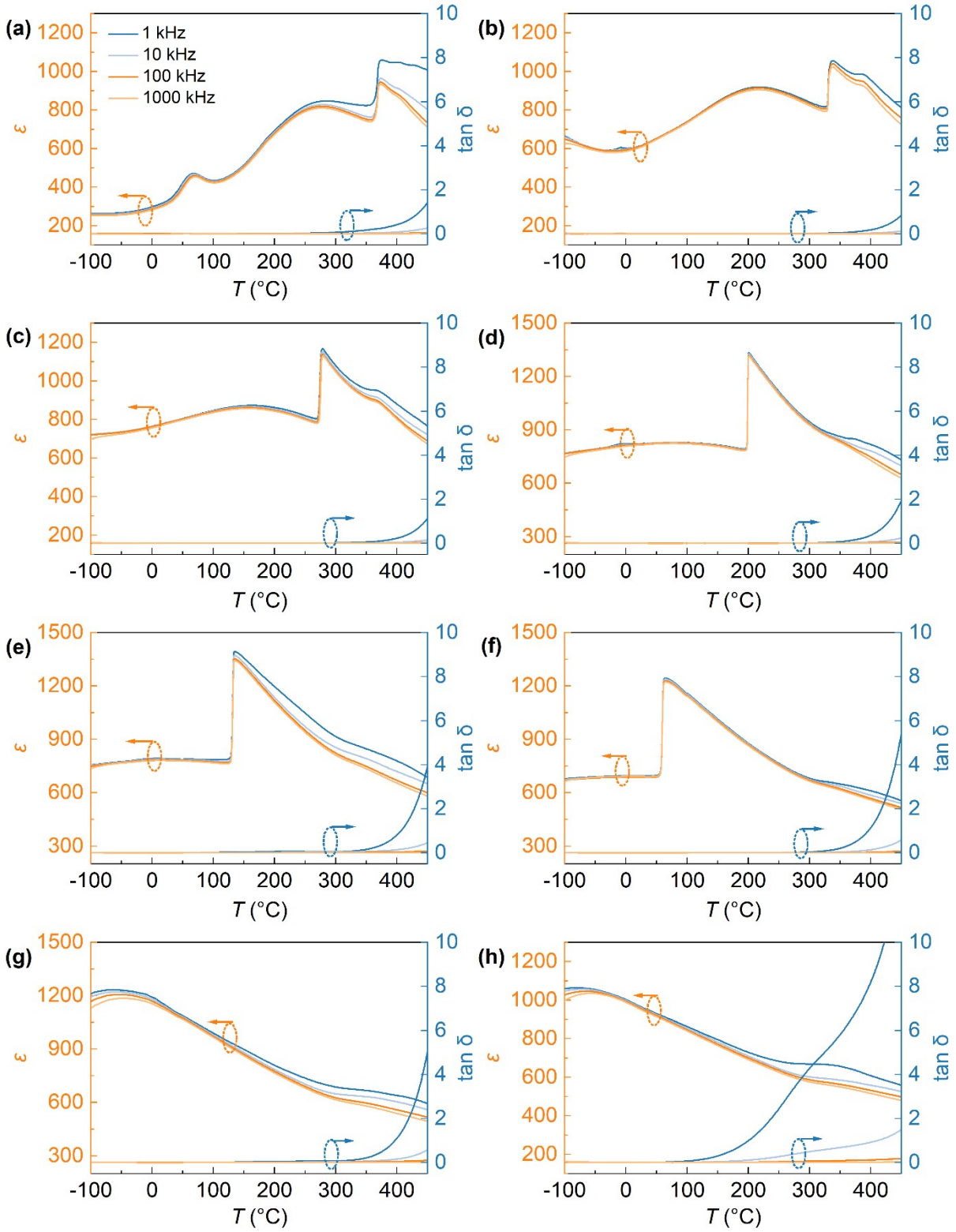

Fig. S6 Temperature dependence of dielectric constant and dielectric loss measured at various frequencies during the heating process from -100 to 450 °C. (a) AN-0.00Bi; (b) AN-0.02Bi; (c) AN-0.04Bi; (d) AN-0.06Bi; (e) AN-0.08Bi; (f) AN-0.10Bi; (g) AN-0.12Bi and (h) AN-0.14Bi ceramics.

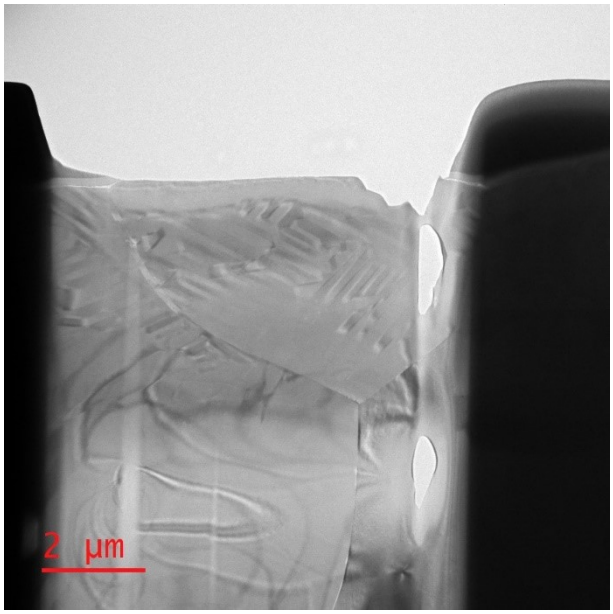

Fig. S7 Overview bright-field TEM image of AN-0.12Bi ceramic.

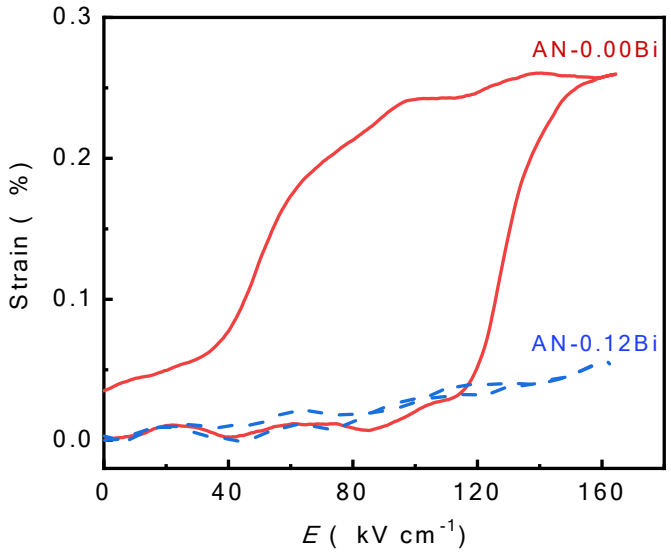

Fig. S8 The electric-field-induced strain of AN-0.00Bi and AN-0.12Bi ceramics.

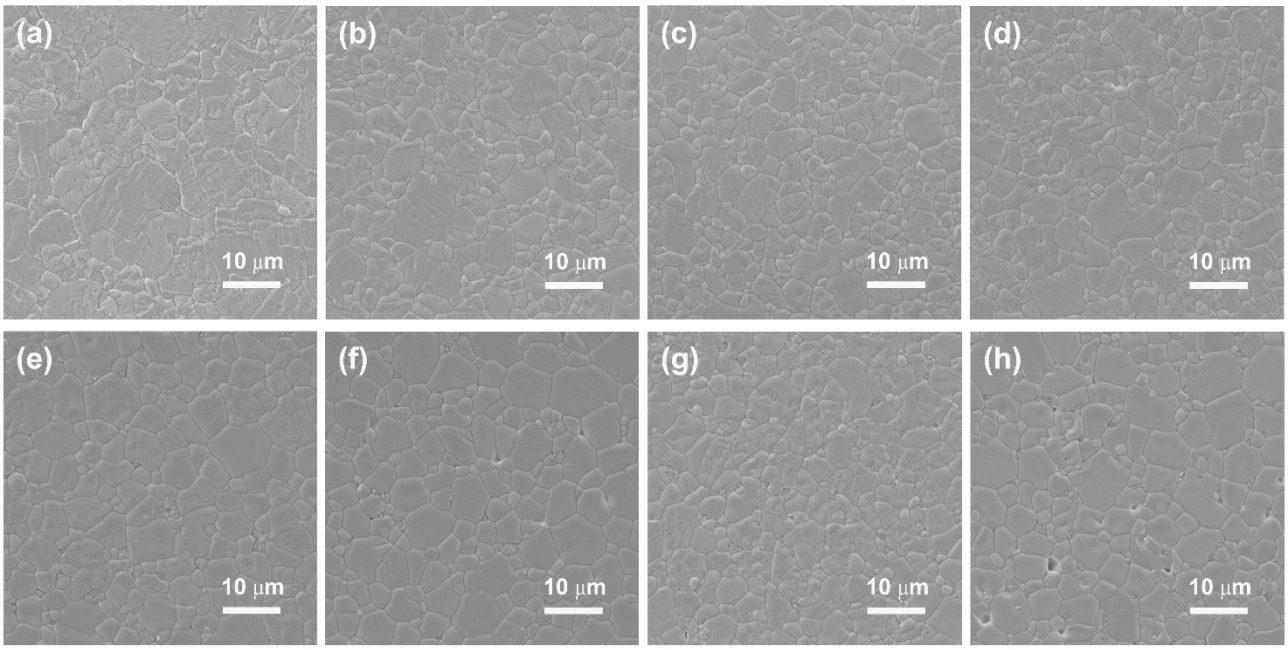

Fig. S9 SEM images of AN-*x*Bi ceramics: (a) *x*=0.00, (b) *x*=0.02, (c) *x*=0.04, (d) *x*=0.06, (e) *x*=0.08, (f) *x*=0.10, (g) *x*=0.12 and (h) *x*=0.14.

The strain, which would cause electromechanical breakdown, may be also responsible for the sharply changed E_b in AN-*x*Bi ceramics. As there is a quadratic relationship between strain and polarization, the strain jump occurs over very small electric field range and thus increases the risk of mechanical failure in dielectric materials with square-shaped *P*-*E* loops, while the strain normally develops slowly over a wide external electric field range in the ones with slim-slanted hysteresis loops (J. Appl. Phys. 2016, 119, 024104). This should be evident in present work. Take two representative samples, revealing nearly square-shaped *P*-*E* loops (i.e., AN-0.00Bi) and slim-slanted *P*-*E* loops (i.e., AN-0.12Bi), for example. The electric-field-induced strain of AN-0.00Bi and AN-0.12Bi displayed giant difference at the same electric field of 165 kV cm^{-1} (Fig. S8). Though this trend does not fit the *x*=0.14 sample, the decreased E_b here is attributed to a porous microstructure, as shown in Fig. S9.

Table S1 The comparison on the energy storage properties between our present work and representative lead-based AFE ceramics

Sample	Energy storage properties obtained via *P-E* loops			Overdamped discharge energy density		Preparation method	Reference
	W_{rec} (J cm^{-3})	η (%)	Electric filed (kV cm^{-1})	W_d (J cm^{-3})	Electric filed (kV cm^{-1})		
0.10 wt% MnO_2-$Ag_{0.64}Bi_{0.12}NbO_3$ (AN-0.12Bi)	9.0	90	650	8.0	600	Solid-state reaction	This work
$0.99(Pb_{0.97}La_{0.02})(Zr_{0.6}Sn_{0.4})O_3$-$0.01AgNbO_3$	10.81	85.05	400	8.72	360	Solid-state reaction	J. Mater. Chem. A 2021, 9, 11291
$Pb_{0.88}La_{0.04}Sr_{0.06}((Zr_{0.6}Sn_{0.4})_{0.84}Ti_{0.16})O_3$	1.52	93.3	129	1.21	129	Solid-state reaction	Ceram. Int. 2016, 42, 12875
$(Pb_{0.915}Ba_{0.04}La_{0.03})(Zr_{0.65}Sn_{0.3}Ti_{0.05})O_3$	4.44	88.8	170	4.22	170	Solid-state reaction	Ceram. Int. 2020, 46, 18106
$(Pb_{0.965}Sr_{0.02}Bi_{0.01})(Zr_{0.6}Sn_{0.4})O_3$	11.28	85.54	350	7.6	350	Solid-state reaction	Chem. Eng. J. 2022, 434, 134660

$(Pb_{0.97}La_{0.02})(Zr_{0.8}Sn_{0.145}Ti_{0.055})O_3$	4.38	70	~250	\	\	Solid-state reaction	Ceram. Int. 2017, 43, 11428
$(Pb_{0.955}La_{0.03})(Zr_{0.5}Sn_{0.43}Ti_{0.07})O_3$	4.2	78	~200	\	\	Solid-state reaction	Ceram. Int. 2019, 45, 11375
$0.92Pb(Tm_{1/2}Nb_{1/2})O_3$-$0.08Pb(Mg_{1/3}Nb_{2/3})O_3$	3.12	\	~310	\	\	Solid-state reaction	J. Eur. Ceram. Soc. 2017, 37, 3329
$(Pb_{0.93}Ba_{0.04}La_{0.02})(Zr_{0.65}Sn_{0.3}Ti_{0.05})O_3$-$0.005Mn_2O_3$	2.64	73	308	\	\	Solid-state reaction	J. Am. Ceram. Soc. 2019, 102, 1912
$Pb_{0.98}La_{0.02}(Hf_{0.45}Sn_{0.55})_{0.995}O_3$	7.63	94	380	\	\	Rolling process	J. Mater. Chem. C 2020, 8, 17016
$Pb_{0.94}La_{0.02}Sr_{0.04}(Zr_{0.9}Sn_{0.1})_{0.995}$	11.18	82.2	395	8.6	400	Tape-casting	J. Mater. Chem. A 2019, 7, 11858
$Pb_{0.95}Ca_{0.02}La_{0.02}(Zr_{0.93}Sn_{0.05}Ti_{0.02})O_3$	14.5	77.1	448	11.6	448	Tape-casting	J. Eur. Ceram. Soc. 2021, 41, 4138
$(Pb_{0.96}La_{0.04})(Zr_{0.99}Ti_{0.01})O_3$	11.38	79.2	395	6.2	350	Tape-casting	ACS Appl. Energy Mater. 2021, 4, 4897

$(Pb_{0.94}Sm_{0.04})(Zr_{0.6}Sn_{0.4})O_3$	11.2	85.1	400	9.7	410	Tape-casting	Chem. Eng. J. 2022, 447, 137367
$(Pb_{0.88}Cd_{0.03}La_{0.06})(Zr_{0.6}Sn_{0.4})O_3$	19.3	91	870	15.35	780	Tape-casting	Adv. Mater. 2022, 34, 2201333
$Pb_{0.98}La_{0.02}(Zr_{0.7}Sn_{0.3})_{0.995}O_3$	12.6	80	560	3.7	300	MLCC	Inorg. Chem. Front. 2020, 7, 756